

# Facile Recycling Strategy of Dyed Polyester Waste by Template-Based Synthesis of UiO-66 for Value-Added Transformation into Self-detoxifying Fabrics

Seokhee Chang, Soyeon Jin, and Jooyoun Kim\*

Cite This: *ACS Omega* 2024, 9, 15074–15084

Read Online

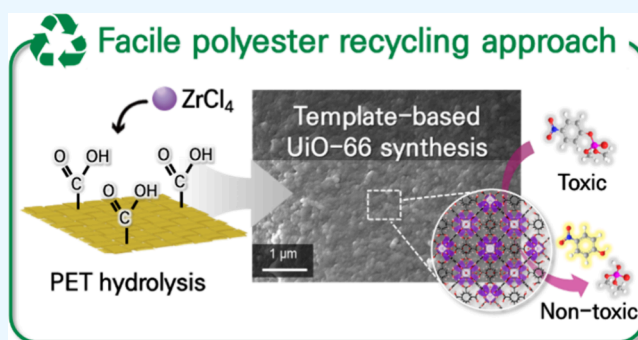
ACCESS |

Metrics &amp; More

Article Recommendations

Supporting Information

**ABSTRACT:** Polyethylene terephthalate (PET) accounts for a significant portion of textile waste, and recycling strategies for this material have attracted much attention. This study proposes a facile and innovative PET recycling method applicable to environmental remediation that involves the conversion of dyed PET fabric waste into a value-added fabric. Herein, a template-based synthesis approach capable of growing a UiO-66 metal–organic framework (MOF) directly on a dyed PET fabric is reported. The advantage of this process lies in its simplicity, where the partial hydrolysis of PET followed by a zirconium chloride treatment results in the successful growth of UiO-66 on a dyed PET fabric with the concurrent removal of the dye without additional steps. The catalytic performance of the UiO-66-grown fabric was evaluated through the degradation of dimethyl 4-nitrophenyl phosphate (DMNP), a nerve agent simulant. The fabric produced by the simple metal treatment ( $\text{Zr@PET}_{\text{hyd}}$ ) exhibited excellent DMNP degradation performance with  $t_{1/2} = 43.3$  min and maintained functional stability after a harsh washing procedure, an outcome attributed to the surface-assisted UiO-66 growth that ensured good bonding stability. The developed process is innovative in that it uses dyed PET waste as a template for the direct growth of UiO-66, simplifying the process without compromising the catalytic functionality. This research provides an informative option for a sustainable textile recycling strategy by transforming dyed PET waste into an advanced self-detoxifying material.



## INTRODUCTION

Polyethylene terephthalate (PET) is widely used in everyday plastics and textiles, and environmental issues related to PET waste disposal have led to significant concerns.<sup>1,2</sup> Among PET recycling approaches, chemical recycling is attracting attention due to its versatility in yielding a wide range of distinct materials.<sup>3,4</sup> As terephthalic acid (TA) is both a monomeric component of PET and a ligand of certain metal–organic frameworks (MOFs) at the same time, efforts have been made to obtain TA from PET waste and use it as a MOF synthesis ingredient.<sup>5–7</sup> MOFs, gaining increasing attention in the environment and energy sectors, are composed of metal clusters and organic ligands, forming porous crystals with a high surface area and numerous catalytic sites.<sup>8–10</sup> Among the wide range of applications, MOFs have emerged as highly efficient catalysts, with the metal-containing building units acting as a Lewis acid for catalyzing the hydrolysis of hazardous compounds.<sup>11,12</sup> In particular, Zr-based MOFs have been applied to decompose organophosphorus chemical warfare agents (CWAs), effectively cleaving the phosphate ester bond at the Lewis acidic sites on Zr<sup>6</sup> nodes.<sup>13–15</sup>

In many cases, MOFs are used as a composite form for practical applications.<sup>16–18</sup> In this regard, extensive studies are

underway to develop textile-based MOF composites for a wide range of potential applications.<sup>19,20</sup> Specifically, the fabrication process from PET waste to MOF-based textiles involves additional steps, such as extracting TA, the synthesis of MOF, and application to a substrate, making the process even more laborious.<sup>21</sup> Meanwhile, the complete decomposition of PET fabrics into a powdery form of TA appears somewhat wasteful, as the fabric itself can be used as a substrate for MOF attachment. Thus, it is necessary to design a simplified recycling process to turn PET waste into MOF-treated textiles without completely sacrificing the fabric structure. Such an advance can help to expand PET recycling opportunities.

Recently, exploratory research was conducted to use PET as a template to grow a TA-based MOF, proposing a method for the direct preparation of MOF-grown materials.<sup>22–24</sup> For this procedure, PET is partially hydrolyzed to reveal carboxyl

Received: November 21, 2023

Revised: March 4, 2024

Accepted: March 14, 2024

Published: March 22, 2024



functional groups on its surface, with these functional groups acting as nucleation sites for the direct bonding with metal ions.<sup>25</sup> While it is expected that the extent of available carboxyl groups affects MOF synthesis, more clarification is needed with regard to how the hydrolysis condition and TA ligand concentration affect MOF growth.<sup>26</sup> Moreover, previous studies<sup>22–24</sup> of template-based MOF growth focused on the use of transparent, dye-free bottle-grade PET as a substrate. However, it is important to note that over 60% of PET is used in synthetic fibers and textiles, which often contain dyes and other additives.<sup>27</sup> Decomposing dyed PET without dye removal can leave residual dye in the TA, which may impede the coordination process during MOF synthesis, ultimately affecting the crystallization of MOFs.<sup>6</sup> Consequently, when dyed PET waste is utilized for MOF synthesis, a proper dye removal procedure is imperative. Specifically, the direct synthesis of MOFs on a dyed PET template requires measures capable of effectively removing dyes while concurrently maintaining the intrinsic chemical and physical structure of the PET.

Herein, a simple process of synthesizing UiO-66 directly onto dyed PET textile waste, denoted as a template-based approach, is introduced. In this procedure, the PET surface was partially hydrolyzed to expose carboxyl groups, and metal ions were treated so that they could bond to the exposed carboxylates. During this procedure, acid hydrolysis was employed to decompose the chromophoric groups of the dyes in the PET. Simultaneously, the surfaces of the PET fibers were functionalized with carboxyl groups to facilitate bonding with metal ions for the synthesis of UiO-66. DMF was used as a solvent in the UiO-66 synthesis process, where it helped to facilitate the removal of residual dye from the PET. The main emphasis of this study is to investigate template-based processability when using the proposed method for the direct synthesis of UiO-66 onto dyed PET as a novel upcycling strategy for used PET textiles. Variations of the process, including the hydrolysis conditions and an external addition of TA, were examined to assess the functional effectiveness and durability of the resulting material upon degrading dimethyl 4-nitrophenyl phosphate (DMNP), a nerve agent simulant. In consideration of practical applicability, the cyclic stability and functional durability of the developed material were evaluated by examining the effects of hydrolysis on the bonding stability. This study attempted to maximize the process efficiency to develop a value-added MOF textile from textile waste, thereby widening the value-added recycling window. As dyed PET textiles constitute the majority of waste PET waste, this study employed dyed PET textile waste for conversion to a detoxified fabric, anticipating the demonstration of a practical upcycling strategy.

## MATERIALS AND METHODS

**Materials.** PET fabrics dyed with anthraquinone dye (AISE-30) were purchased from Testfabrics, Inc. (West Pittston, PA, USA). Nitric acid (HNO<sub>3</sub>, 70%), toluidine blue O (TBO), zirconium(IV) chloride anhydrous (ZrCl<sub>4</sub>), *N,N*-dimethylformamide (DMF), hydrochloric acid (HCl), terephthalic acid (TA), ethanol, and acetic acid were purchased from Daejung Chemicals (Gyeonggi-do, Korea). *N*-Ethylmorpholine (NEM) (97%), *p*-nitrophenoxide (≥98%), and dimethyl 4-nitrophenyl phosphate (DMNP, ≥98%) were purchased from Sigma-Aldrich (St. Louis, MO).

**Hydrolysis of PET Fabrics.** PET fabrics were cut into 3 × 3 cm. Then, 5 g of fabric was immersed in 300 mL of 7 M HNO<sub>3</sub> aq. solution. The mixture was heated with a reflux condenser at 90 °C for 5 h. After the reaction, the fabric was taken out to rinse with distilled water and oven-dried at 40 °C for 24 h. The same protocol was applied with varied reaction time from 1 to 6 h to determine the optimal hydrolysis condition.

**Synthesis of UiO-66-Grown PET Fabrics.** As shown in Table 1 and Figure 1, the UiO-66-treated fabrics were

**Table 1. Samples of UiO-66-Grown PET Fabrics**

sample	PET treatment	UiO-66 synthesis method
Zr@PET <sub>hyd</sub>	hydrolyzed	ZrCl <sub>4</sub> was treated onto hydrolyzed fabric.
Zr+TA@PET <sub>hyd</sub>	hydrolyzed	ZrCl <sub>4</sub> and additional TA were treated onto hydrolyzed fabric.
Zr@PET	untreated	ZrCl <sub>4</sub> was treated onto untreated fabric.
Zr+TA@PET	untreated	ZrCl <sub>4</sub> and additional TA were treated onto untreated fabric.

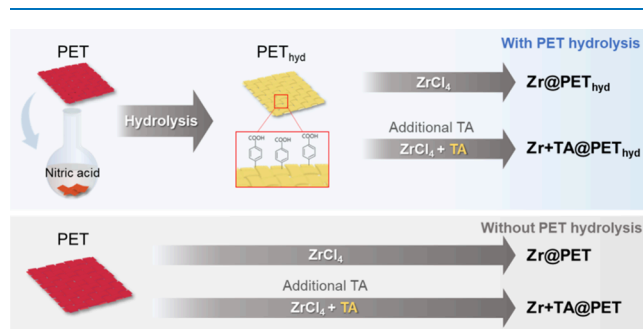


**Figure 1.** Synthesis of Zr@PET<sub>hyd</sub>, Zr+TA@PET<sub>hyd</sub>, Zr@PET, and Zr+TA@PET.

prepared by four different methods, varying the PET hydrolysis and extra TA addition. For the preparation of Zr@PET<sub>hyd</sub>, the hydrolyzed PET was treated with DMF to facilitate the complexation of zirconium ions by releasing free TA from hydrolyzed PET. A 1 g of hydrolyzed PET fabrics (3 cm × 3 cm) was immersed in a vial containing 20 mL of DMF, heated up to 120 °C for 12 h, and then cooled to room temperature. The metal precursor solution was prepared by adding 0.375 g of ZrCl<sub>4</sub> in a mixed solvent consisting of 5 mL of DMF and 3 mL of HCl. The metal precursor solution was added to the vial containing PET fabrics and DMF, and then the solution was sonicated for 20 min. After sonication, the solution and the fabric were heated up to 80 °C for 24 h.

For Zr+TA@PET<sub>hyd</sub>, supplementary TA was added in Zr treatment. The DMF process of the hydrolyzed PET fabric was conducted identically with Zr@PET<sub>hyd</sub>. The ligand precursor solution was prepared by adding 0.267 g of TA in 5 mL of DMF. 8 mL of ZrCl<sub>4</sub> solution prepared as above and 5 mL of TA/DMF solution were added together into the vial containing PET fabric and DMF. The mixture was sonicated for 20 min and placed in the oven at 80 °C for 24 h.

The Zr+TA@PET sample was prepared the same way as Zr+TA@PET<sub>hyd</sub> except that the treatment was conducted on an untreated (nonhydrolyzed) PET fabric. For Zr@PET, the untreated (nonhydrolyzed) PET fabric was immersed in 20 mL of DMF without heating; then, the metal precursor was added to it, with 20 min of sonication and then heating at 80

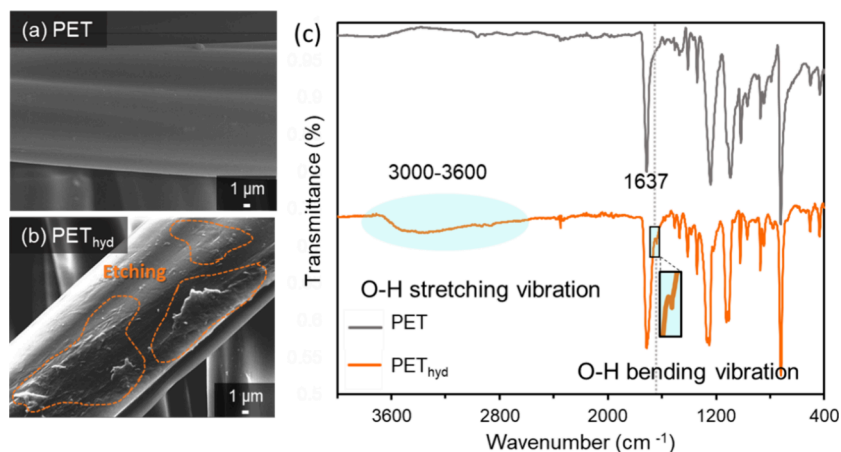


**Figure 2.** FE-SEM image of (a) PET and (b) PET<sub>hyd</sub>. (c) FTIR spectra of PET and PET<sub>hyd</sub>.

°C for 24 h. After synthesis, all samples were washed in DMF and ethanol and then oven-dried at 40 °C for 24 h.

Additionally, powdery UiO-66 was fabricated via the solvothermal method as follows: 0.375 g of ZrCl<sub>4</sub> and 0.267 g of TA were dissolved in 30 mL of DMF under sonication. Then, the solution was heated at 80 °C for 24 h. After cooling in air to room temperature, the resulting UiO-66 was washed with DMF and ethanol and then oven-dried at 40 °C for 24 h.

**Characterization.** Morphologies of fabric samples were observed by field emission scanning electron microscopy (FE-SEM) (JSM-7800F Prime, JEOL Ltd., Tokyo, Japan) with prior treatment with Pt sputter-coating under 20 mA for 180 s (108 Auto Sputter Coater, Ted Pella, CA, USA) and corrected scanning transmission electron microscopy (Cs-TEM) (JEM-ARM200F, JEOL Ltd., Tokyo, Japan). Elemental mapping was done by energy-dispersive spectroscopy (EDS) equipped with a NORAN system 7 detector (ThermoFisher Scientific, Waltham, MA, USA) attached to the FE-SEM. For analysis of the crystalline phase of powdery UiO-66 and the fabric sample, high resolution X-ray diffraction (HRXRD) (SmartLab, Rigaku Corp., Tokyo, Japan) with a Cu-targeted X-ray generator was used. The chemical composition of material was analyzed by the Fourier transform infrared-attenuated total reflectance spectroscopy (FTIR-ATR) (Tensor27, Bruker Corp., MA, USA) in 400 to 4000 cm<sup>-1</sup>. Brunauer–Emmett–Teller (BET) adsorption analysis was conducted for fabricated samples by the nitrogen (N<sub>2</sub>) sorption–desorption isotherm (Tristar II 3020, Micromeritics, USA). The samples were degassed at 373 K for 12 h under vacuum, and then N<sub>2</sub> gas (99.99%) was purged at 77 K. BET surface area was calculated in the relative pressure range of 0.0 to 1.0 bar.

The concentration of Zr in the fabricated samples was analyzed using inductively coupled plasma optical emission spectroscopy (ICP-OES) (ICP5800, Agilent Technologies, CA, USA). Before the analysis, the samples were treated with HNO<sub>3</sub> (2.5 mL) and HCl (7.5 mL), heated to 200 °C, and kept at this temperature for 3 h. Following the decomposition of the samples, the solution was filtered through 0.45 μm syringe filters.

Zr element leaching was measured by inductively coupled plasma mass spectrometry (ICP-MS) (Varian 820-MS, Varian, Melbourne, Australia). UV/vis absorption spectra of 4-nitrophenol was analyzed using the UV/vis spectrometer (UV-2600, Shimadzu, Japan). Tensile strength of fiber samples (2.5 × 15 cm) was evaluated using a universal testing machine

(SST, Tinius Olsen, Redhill, England). A crosshead speed of 150 mm·min<sup>-1</sup> and gauge length of 100 mm was used for the test.

**DMNP Hydrolysis Test.** The pH of 0.45 M aq. N-ethylmorpholine (NEM) solution was adjusted to pH 9 with addition of acetic acid.<sup>28,29</sup> A 60 mg sample of fabric cut in 0.3 cm × 0.3 cm was immersed in 1.5 mL of prepared NEM solution, and the solution was stirred at 1100 rpm for 30 min. Then, 4 μL of DMNP was added to this fabric-containing solution with continuous stirring. The DMNP conversion (%) was monitored by measuring the concentration of conversion intermediate, *p*-nitrophenoxide. A 10 μL portion of the reaction solution was diluted in 3 mL of 0.45 M aq. NEM solution, and the absorbance was measured at 403 nm to measure the concentration of *p*-nitrophenoxide. All tests were performed under dark conditions. For the cyclic stability test, the used fabric was washed sequentially with ethanol and distilled water after each hydrolysis test and dried at 40 °C for 12 h to remove any residual solvent.

**Quantitative Measurement of –COOH from the Surface.** The number of carboxyl groups exposed on the PET fabric was determined by surface derivatization with toluidine blue O (TBO).<sup>30</sup> A fabric in 3 cm × 3 cm was incubated in 10 mL of 0.5 mM TBO aq. solution at 30 °C for 6 h, adjusting the solution pH to 10 using NaOH. After 6 h of incubation, the fabric was washed with 0.1 mM aq. NaOH for 10 min to remove free TBO. Then, the surface-bound TBO was released by immersing the fabric in 5 mL of 17.5 M acetic acid aq. solution for 30 min. The amount of detached TBO was measured by UV/vis spectroscopy at 630 nm, and the surface density of carboxyl groups was calculated by assuming that each carboxyl group is bonded to a single TBO molecule.

**Dye Removal Analysis.** The color strength (*K/S*) values of PET fabrics were measured on a spectrophotometer (CM-26d, Konica Minolta, Japan). *K/S* values represent the ratio of light absorbed to light reflected by the fabric. Dye removal (%) of fabrics was calculated by eq 1, where [*K/S*]<sub>A</sub> is the *K/S* value of dyed PET, [*K/S*]<sub>B</sub> is the *K/S* value of undyed white PET, and [*K/S*]<sub>C</sub> is the *K/S* value of dyed fabric that is hydrolyzed or has undergone both hydrolysis and DMF-assisted solvothermal UiO-66 synthesis.

$$\text{dye removal}(\%) = \frac{[K/S]_A - [K/S]_C}{[K/S]_A - [K/S]_B} \times 100 \quad (1)$$

**Durability Test.** To test the functional durability, a fabric sample in 3 cm × 3 cm was washed in ethanol stirring at 300 rpm for 24 h. The sample was dried at 40 °C for 12 h, and DMNP hydrolysis tests were conducted to assess the performance after the washing procedure.

## RESULTS AND DISCUSSION

### PET Hydrolysis with Various Treatment Times.

Throughout the experiments, PET fabric materials dyed with a red disperse dye was used. While the PET fabric displayed a smooth surface, hydrolyzed PET (PET<sub>hyd</sub>) showed an etched surface (Figures 2a,b). From FTIR spectra of the untreated and hydrolyzed PET fabrics (Figure 2c), typical PET peaks appeared from 1241, 1339, 1408, and 1712 cm<sup>-1</sup>, corresponding to the stretching vibrations of C–O–C, C–O, C–C, and C=O, respectively.<sup>31</sup> After hydrolysis (PET<sub>hyd</sub>), peaks at 3000–3600 and 1637 cm<sup>-1</sup> newly appeared, corresponding to O–H stretching vibration and O–H bending vibration, respectively.<sup>32,33</sup> An XPS analysis confirmed an increased percentage of O at the surface after hydrolysis due to formation of –COOH and –OH groups on the PET surface (Table 2).<sup>34</sup>

**Table 2.** XPS Atomic Compositions of PET and PET<sub>hyd</sub> Surfaces

sample	atomic composition (%)	
	C	O
PET	73.6	26.4
PET <sub>hyd</sub>	71.7	28.3

In Figure 3a, PET tensile strength results with various hydrolysis times are shown. Compared to an untreated PET fabric sample for which the tensile strength was 544 N, the tensile strength of PET<sub>hyd</sub> dropped by more than 55% after 1 h of hydrolysis (246 N), with the strength continuing to decrease as the hydrolysis time increased. As a reference sample, the tensile strength of a useful spunbond nonwoven fabric with a basis weight of 29 g·m<sup>-2</sup> was measured and found to be 59 N. As 6 h of hydrolysis of the sample (PET<sub>hyd</sub>\_6h) weakened the fabric, with a resulting value as low as 31 N, hydrolysis to this extent was excluded from further experiments.

Given that the purpose of hydrolysis is to realize reactive carboxyl groups at the surface, the carboxyl group density with longer hydrolysis times was investigated by a TBO assay.<sup>35,36</sup> As shown in Figure 3b, PET<sub>hyd</sub> with an increased hydrolysis time resulted in a higher density of the carboxyl groups, which will act as metal-binding sites. The PET fabric hydrolyzed for 5 h (PET<sub>hyd</sub>\_5h) displayed higher carboxyl surface density (31 nmol·cm<sup>-2</sup>) by approximately 60% compared to the untreated PET fabric. When the hydrolyzed PET was treated with a ZrCl<sub>4</sub> solution, UiO-66 was directly grown on the PET fabric (Zr@PET<sub>hyd</sub>). Assuming that the increased carboxyl surface density would lead to a greater amount of UiO-66 synthesis, the carboxyl surface density can be associated with the extent of the catalytic reaction that leads to DMNP degradation. In Figure 3c, the degradation of DMNP (for 240 min) represented by the DMNP absorbance ( $\lambda_{\text{max}} = 273$  nm) was examined for Zr@PET<sub>hyd</sub> at different PET hydrolysis times. As expected, the DMNP absorbance decreased as the hydrolysis time was increased, implying that a longer hydrolysis time results in a greater amount of UiO-66 synthesis, eventually demonstrating higher DMNP degradation performance.<sup>37</sup>

To quantify the DMNP degradation, the absorbance peak of *p*-nitrophenoxide, an intermediate product during the DMNP degradation process (Figure 3e), is generally used, as the absorbance peak of *p*-nitrophenoxide is linearly correlated with the extent of DMNP degradation.<sup>38</sup> In other words, as DMNP degrades, it is converted more into *p*-nitrophenoxide. In this study, a higher DMNP conversion rate (%) indicates relatively more *p*-nitrophenoxide produced from a greater extent of DMNP degradation.<sup>39</sup> A further analysis of DMNP degradation was conducted by measuring the absorbance of *p*-nitrophenoxide. In Figure 3d, the DMNP conversion of Zr@PET<sub>hyd</sub> is shown to have increased as the hydrolysis time was increased, suggesting that the greater carboxylic density, attributed to the extended hydrolysis period, allowed a higher loading of UiO-66, leading to an enhanced catalytic reaction for DMNP degradation.

**Fabrication of UiO-66-Grown Fabrics.** As illustrated in Table 1 and Figure 1, UiO-66-grown fabrics were synthesized by four different methods. The treatments of particular interest are denoted here as Zr@PET<sub>hyd</sub> and Zr+TA@PET<sub>hyd</sub>, anticipated to form UiO-66 directly on a hydrolyzed PET substrate. For Zr+TA@PET<sub>hyd</sub>, the effect of a supplementary TA addition on the UiO-66 synthesis process was analyzed. As a comparison, the Zr+TA@PET sample was prepared by a typical MOF treatment method, where PET without hydrolysis was treated with ZrCl<sub>4</sub> and TA. The Zr@PET sample, a control sample here, is used to examine whether a single treatment of ZrCl<sub>4</sub> on PET (without hydrolysis) forms any UiO-66 on the surface. From the morphological observation in Figure 4a, Zr@PET showed no specific features on the surface, indicating that the MOF was not synthesized by the single treatment of ZrCl<sub>4</sub> on a PET fabric. Without hydrolysis, Zr ions did not attach to the inert PET surface. The hydrolyzed PET, on the other hand, exhibited uniform crystal growth on the surface with the same ZrCl<sub>4</sub> treatment, as shown by Zr@PET<sub>hyd</sub> in Figure 4d. A difference was observed during the reaction of Zr@PET and Zr@PET<sub>hyd</sub>, during which white precipitates formed from the Zr@PET<sub>hyd</sub> reaction, whereas the Zr@PET reaction solution remained transparent (Figure S1). After hydrolysis, the PET surface is uniformly carboxylated with metal ions chemically bonded to form UiO-66. However, UiO-66 at the outermost layer may be physically adhered, resulting in a reduced bonding strength. Figure S2 presents the uniform formation of UiO-66 on Zr@PET<sub>hyd</sub>, as shown from the uniform coverage of the elemental mapping for C, O, and Zr. From the cross-sectional TEM image, a thin MOF layer is apparent from Zr@PET<sub>hyd</sub> (~74 nm), indicating the uniform synthesis of UiO-66 on the PET surface (Figure 4e).

With the addition of supplementary TA to the ZrCl<sub>4</sub> solution, both Zr+TA@PET and Zr+TA@PET<sub>hyd</sub> showed substantial loading of MOF aggregates (Figure 4b,c). Also, the same types of precipitates formed within the reaction solution for those samples (Figure S1). For Zr+TA@PET without the hydrolysis of PET, the surface is inert and thus chemical bonding with Zr ions does not occur. Instead, UiO-66 formed in solution can physically attach onto random sites on the PET surface. Once nucleation seeds are formed randomly on the PET surface, more of UiO-66 can be physically attached, leading to aggregation.<sup>40</sup> Consequently, Zr+TA@PET showed poor coverage of UiO-66 on the fiber surface compared to the sample treated on the hydrolyzed PET (Figure 4b). For the hydrolyzed sample, Zr+TA@PET<sub>hyd</sub>, MOFs were rather

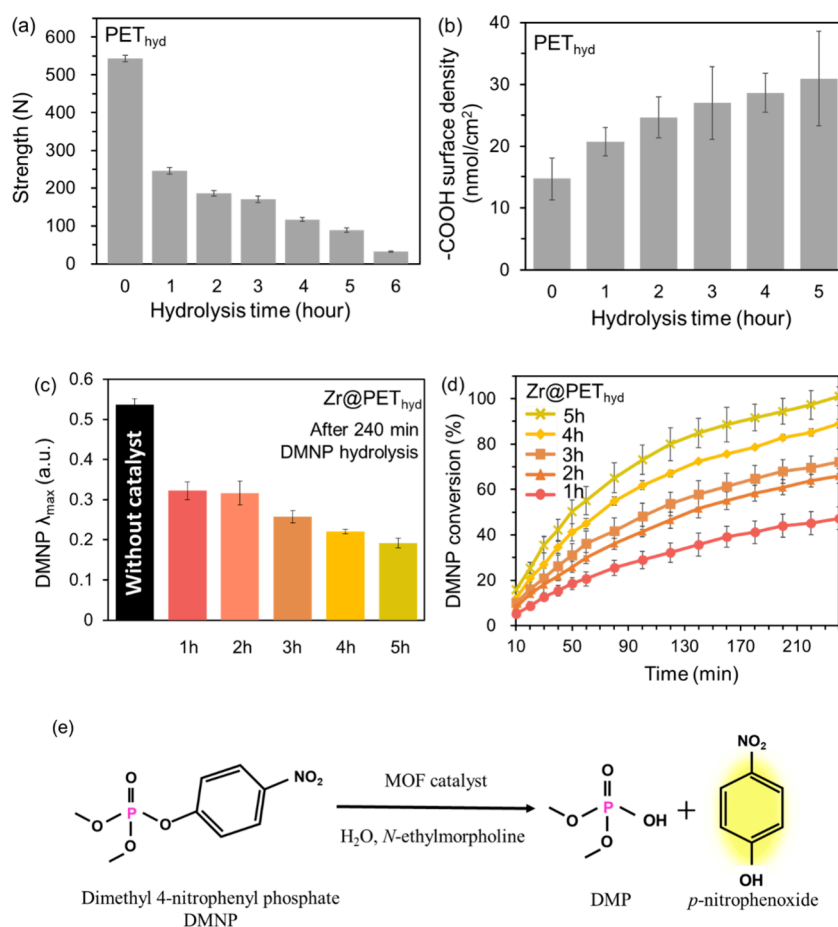


**Figure 3.** (a) Tensile strength of hydrolyzed PET (PET<sub>hyd</sub>), (b) surface carboxylic density on PET<sub>hyd</sub>, (c) DMNP  $\lambda_{\text{max}}$  (273 nm) of Zr@PET<sub>hyd</sub> after DMNP hydrolysis for 240 min, and (d) DMNP conversion into *p*-nitrophenoxide (%) by Zr@PET<sub>hyd</sub>, measured by the absorbance of *p*-nitrophenoxide. (e) DMNP hydrolysis mechanism by UiO-66.

uniformly grown on the fiber surface, which is attributed to -COOH sites from the hydrolyzed surface.

In Figure 4f, from the X-ray diffraction (XRD) analysis, broad diffraction peaks corresponding to crystalline PET are observed from all samples, confirming that neither the hydrolysis process nor MOF growth changed the crystal structure of PET. The Zr+TA@PET<sub>hyd</sub> and Zr+TA@PET samples exhibited distinct peaks at 7.4° and 8.5°, corresponding to the (111) and (002) crystal planes of UiO-66.<sup>41</sup> While the peaks for Zr@PET<sub>hyd</sub> were not very clear, subtle protrusions on those positions could be observed. This confirms the presence of UiO-66 on Zr@PET<sub>hyd</sub>, though there is less synthesized UiO-66 compared to the Zr+TA@PET<sub>hyd</sub> and Zr+TA@PET cases, in which additional TA was treated. From the FTIR analysis, Zr@PET<sub>hyd</sub> showed O-H stretching vibration and Zr-O stretching vibration peaks at 3000–3600 and 660 cm<sup>-1</sup>, respectively, confirming the presence of UiO-66 (Figure 4g).<sup>42</sup>

**Dye Removal from PET through Hydrolysis and a DMF Treatment.** The advantage of the developed process is in how dyes are extracted almost completely without additional procedures. Therefore, synthesized UiO-66 demonstrates a performance similar to the performance of UiO-66 manufactured from pure linker and metallic chemicals. Dyes from the PET fabric were removed via acid hydrolysis and the DMF-assisted solvothermal synthesis of UiO-66. As shown in Figure S3, the color of the PET fabric was lightened after each acid

hydrolysis and DMF treatment. The dye removal (%) calculated by eq 1 demonstrates that hydrolysis removed 67.6% of the dye (Table S1). During acid hydrolysis, H<sup>+</sup> ions in the acidic solution facilitate the breakage of the bonds in anthraquinone dyes, degrading the chromophore.<sup>43</sup> Furthermore, the subsequent DMF treatment for the solvothermal synthesis of UiO-66 removed any residual colorant, with a dye removal rate of 98.7% after the combined process of acid hydrolysis and DMF-assisted solvothermal UiO-66 synthesis (Table S1).

This phenomenon can be explained as follows. The Hansen solubility parameter of DMF (24.9) is close to that of PET (22.7), and the relative energy difference (RED) value is as close as 0.95 (Table S2). The lower RED value indicates high affinity between them, implying that DMF can cause substantial swelling of PET.<sup>44</sup> Additionally, because the solvothermal process with DMF was conducted at 120 °C, DMF may have sufficiently swelled the PET fibers, thereby effectively removing the dye from these fibers.

**Catalytic Performance of UiO-66-Grown Fabrics for DMNP Hydrolysis.** As the DMNP hydrolysis proceeded, the absorbance of DMNP ( $\lambda_{\text{max}} = 273$  nm) decreased, while the absorbance of *p*-nitrophenoxide ( $\lambda_{\text{max}} = 403$  nm) increased (Figure 5a–d). As *p*-nitrophenoxide formed, the transparent color of the DMNP solution gradually changed to light yellow.<sup>45</sup> The catalytic effect of the prepared samples for hydrolyzing DMNP was investigated by DMNP conversion

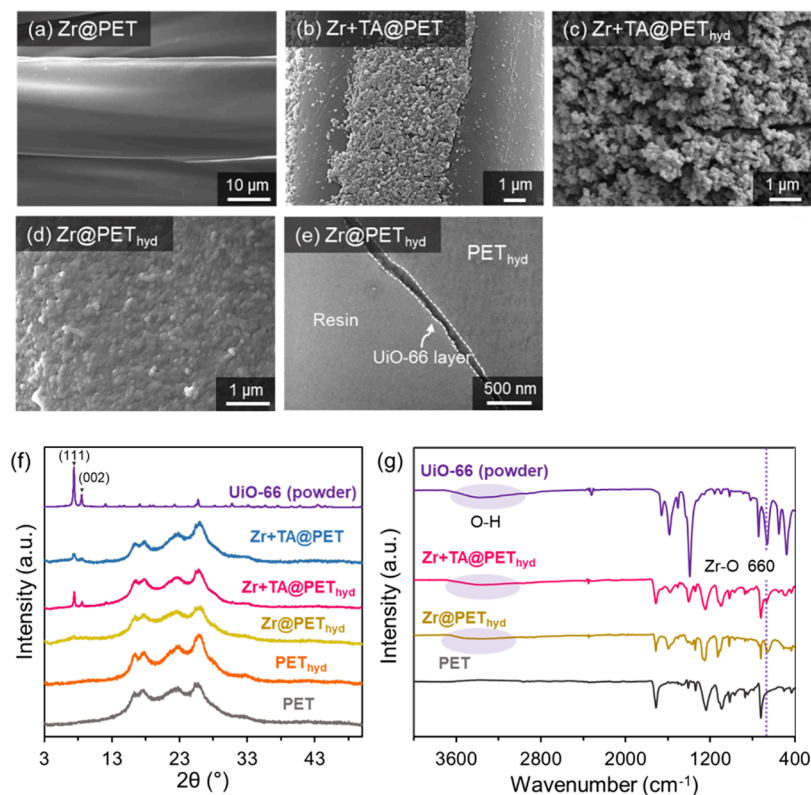


**Figure 4.** Characterization of the fabricated samples. FE-SEM images of (a) Zr@PET, (b) Zr+TA@PET, (c) Zr+TA@PET<sub>hyd</sub>, and (d) Zr@PET<sub>hyd</sub>. (e) TEM image of Zr@PET<sub>hyd</sub> (note: resin used for TEM sample preparation is shown in the image). (f) XRD patterns and (g) FT-IR analysis.

into *p*-nitrophenoxide (%); i.e., the percentage of *p*-nitrophenoxide produced. Figure 5e illustrates that untreated PET and PET<sub>hyd</sub> exhibited negligible conversion rates of 5.4% and 5.5%, respectively, during the 240 min of reaction. The Zr@PET showed very low DMNP conversion of 14.7% for 240 min, aligning with the fact that only a few MOFs were synthesized on the surface, as evidenced in the SEM image in Figure 4a.

The pseudo-first-order rate constant,  $k$ , and the half-life time ( $t_{1/2}$ ) of DMNP conversion, calculated  $t_{1/2} = 0.693/k$ , are compared in Table 3.<sup>46</sup> The results of comprehensive analyses of the first-order kinetics reaction are presented in Figure S4a–e. To examine whether the reactivity of the DMNP conversion was associated with the reactive surface area, the BET surface area and mass ratio of the MOF are also compared (Table 3). The mass ratio of MOF was calculated by eq 2, where  $X$  represents the UiO-66 mass loading (wt %) and  $SA_{UiO+Fiber}$ ,  $SA_{UiO}$ , and  $SA_{Fiber}$  are the BET surface areas ( $m^2 \cdot g^{-1}$ ) of the UiO-66-grown PET, UiO-66, and PET, respectively.<sup>47</sup> It should be noted that the surface areas of PET and PET<sub>hyd</sub> were not measurable by the BET analysis; thus, the surface area of the fabric was considered to be zero in the calculations. Instead, only the surface stemming from UiO-66 was counted. For comparison, powdery UiO-66 had a BET surface area of  $1361.28 m^2 \cdot g^{-1}$ .

$$SA_{UiO+Fiber} = SA_{UiO} + SA_{Fiber} \cdot (1 - X) \quad (2)$$

In the Zr@PET case, for which the MOF loading was negligible, valid BET data were not gained. Zr@PET<sub>hyd</sub>, Zr+TA@PET, and Zr+TA@PET<sub>hyd</sub> showed BET surface areas of 0.54, 12.05, and  $14.55 m^2 \cdot g^{-1}$ , respectively (Table 3 and Figure

S5). The samples synthesized with the addition of an external supplementary TA exhibited relatively high surface areas. This is attributed to UiO-66 particles that grew in multiple layers on the PET surface. In contrast, Zr@PET<sub>hyd</sub> exhibited a relatively low surface area, primarily due to the thin UiO-66 layer on the PET surface with limited TA exposure from the hydrolyzed PET. Similarly, Zr+TA@PET and Zr+TA@PET<sub>hyd</sub>, synthesized with an addition of externally sourced TA, exhibited higher UiO-66 mass loading of 0.89 and 1.07 wt %, respectively, compared to Zr@PET<sub>hyd</sub>, which showed a MOF mass of 0.04 wt %. This result is consistent with the ICP-OES data (Table S3).

In Table 3, the  $t_{1/2}$  outcome for DMNP degradation is listed as shortest to longest in the order of Zr+TA@PET<sub>hyd</sub> (14.5 min) < Zr@PET<sub>hyd</sub> (43.3 min) < Zr+TA@PET (330.0 min) < Zr@PET (1155.0 min). Notably, Zr@PET<sub>hyd</sub> exhibited a significantly shorter  $t_{1/2}$  compared to Zr+TA@PET, despite the fact that Zr+TA@PET had a higher MOF mass (0.89 wt %) than Zr@PET<sub>hyd</sub> (0.04 wt %). In contrast to Zr@PET<sub>hyd</sub>, in which the TA ligand is sourced from the PET substrate, the Zr+TA@PET formed the MOF from the external source of the TA ligand; therefore, the MOF attachment of Zr+TA@PET was rather random on the surface. In the SEM image in Figure 4b, Zr+TA@PET shows partial coverage of UiO-66; as the outermost UiO-66 surface would contribute most to the catalytic reaction,<sup>48,49</sup> the lack of surface coverage by UiO-66 would result in lower catalytic performance. For Zr+TA@PET, the absorbance of DMNP ( $\lambda_{max} = 273$  nm) did not decrease significantly, while that of *p*-nitrophenoxide ( $\lambda_{max} = 403$  nm) increased. It is possible that, for Zr+TA@PET, which had slower catalytic activity, DMNP was partially hydrolyzed to

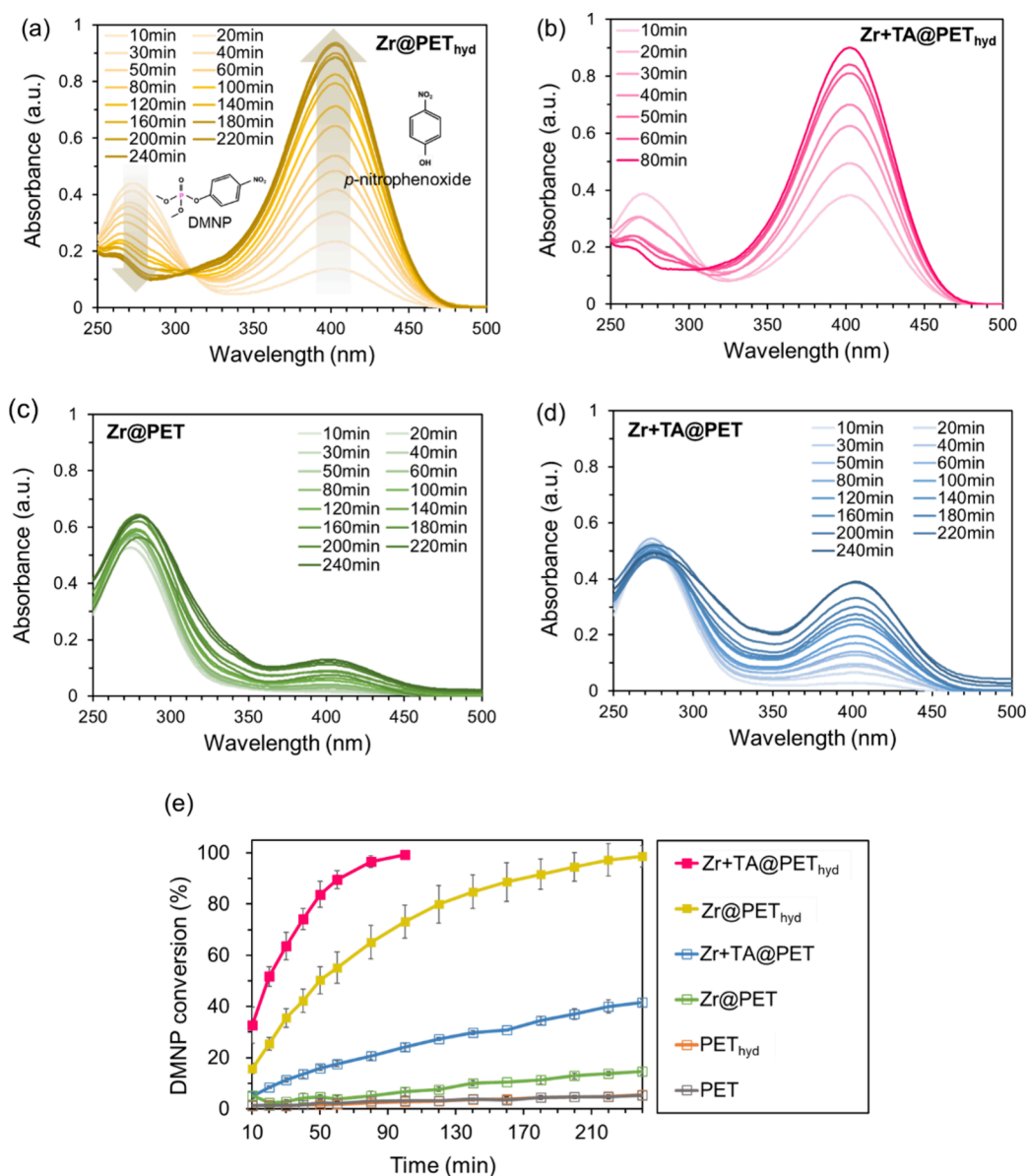


**Figure 5.** UV/vis absorption spectra for monitoring DMNP hydrolysis (a) Zr@PET<sub>hyd</sub>, (b) Zr+TA@PET<sub>hyd</sub>, (c) Zr@PET, and (d) Zr+TA@PET. (e) Conversion of DMNP to *p*-nitrophenoxide for UiO-66-grown fabrics.

**Table 3. Material Characteristics and DMNP Hydrolysis Performance**

sample	BET surface area (m <sup>2</sup> ·g <sup>-1</sup> )	UiO-66 mass loading (wt %)	rate constant, <i>k</i> (min <sup>-1</sup> )	half-life time, <i>t</i> <sub>1/2</sub> (min)
Zr@PET			0.0006	1155.0
Zr+TA@PET	12.05	0.89	0.0021	330.0
Zr@PET <sub>hyd</sub>	0.54	0.04	0.0160	43.3
Zr+TA@PET <sub>hyd</sub>	14.55	1.07	0.0477	14.5

form methyl 4-nitrophenyl phosphate (M4NP) as an intermediate, which has an absorbance peak similar to that of as DMNP at 260–290 nm (Figure 5d).<sup>45,50</sup>

In contrast, Zr@PET<sub>hyd</sub> and Zr+TA@PET<sub>hyd</sub>, which exhibited faster DMNP degradation, showed a significant decrease in the absorbance of DMNP. Specifically, Zr@PET<sub>hyd</sub>

despite the considerably lower loading of UiO-66, had a surface that was fully covered by UiO-66, resulting in a higher catalytic performance. The half-life of the DMNP hydrolysis of Zr@PET<sub>hyd</sub> (43.3 min) is comparable to that of UiO-66 powder (BET surface area of 1450 m<sup>2</sup>·g<sup>-1</sup>), as studied previously by Katz et al.<sup>49</sup> This implies that even with a lower BET surface area, the exposed carboxylic groups on the PET surface allowed the even distribution of MOF growth, resulting in advantageous catalytic performance for DMNP hydrolysis. Though the surface coverage of MOF is a crucial factor affecting the catalytic performance, the higher mass loading of MOF was also advantageous for a fast reaction, as indicated by the highest reaction rate and shortest *t*<sub>1/2</sub> for Zr+TA@PET<sub>hyd</sub>.<sup>51</sup>

From these results, it is evident that MOF formation on a PET substrate is achievable by a simple metal treatment on hydrolyzed PET, even without the addition of an external TA ligand. Moreover, the exposed carboxylic groups on the PET surface allow an even distribution of MOF growth, leading to

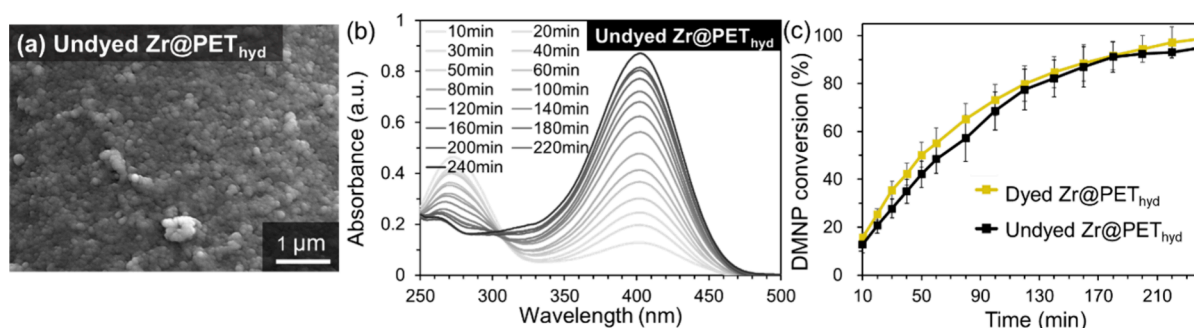


**Figure 6.** (a) FE-SEM image of undyed  $\text{Zr@PET}_{\text{hyd}}$ . (b) UV/vis absorption spectra for monitoring DMNP hydrolysis using undyed  $\text{Zr@PET}_{\text{hyd}}$ . (c) Conversion of DMNP to *p*-nitrophenoxide for dyed and undyed  $\text{Zr@PET}_{\text{hyd}}$ .

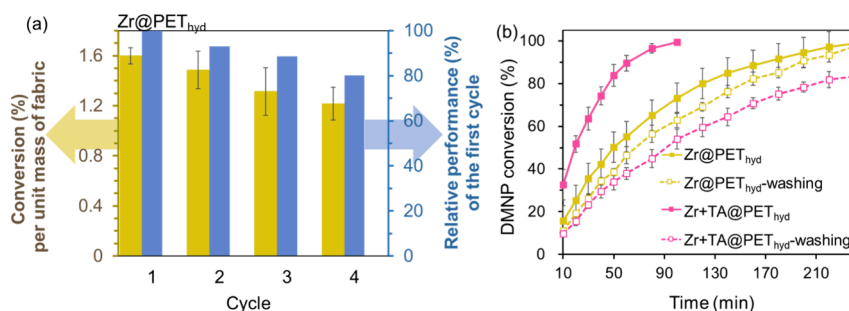


**Figure 7.** (a) Cyclic stability of  $\text{Zr@PET}_{\text{hyd}}$  for conversion of DMNP to *p*-nitrophenoxide. (b) Functional stability of  $\text{Zr@PET}_{\text{hyd}}$  and  $\text{Zr@PET}_{\text{hyd}}$  after harsh washing procedure for 24 h.

advantageous catalytic performance for DMNP hydrolysis. The  $\text{Zr+TA@PET}_{\text{hyd}}$  sample showed the most rapid DMNP degradation, demonstrating that both the uniform distribution and the total mass quantity of MOF affected the catalytic performance.

**Comparison of Dyed and Undyed Fabrics for DMNP Hydrolysis.** To investigate whether the presence of the dye affects the MOF synthesis and the DMNP degradation performance, undyed PET was additionally tested with the same UiO-66 synthesis protocol used with  $\text{Zr@PET}_{\text{hyd}}$ . Figure 6a reveals a morphology similar to that of  $\text{Zr@PET}_{\text{hyd}}$ . For DMNP hydrolysis, the half-life time ( $t_{1/2}$ ) of undyed  $\text{Zr@PET}_{\text{hyd}}$  was 56.3 min, similar to that of  $\text{Zr@PET}_{\text{hyd}}$  (43.3 min) (Figure 6b,c). The comparable degradation performance of dyed and undyed  $\text{Zr@PET}_{\text{hyd}}$  indicates that the dyes initially present on the PET fibers were effectively removed through the processes of acid hydrolysis and solvothermal UiO-66 synthesis. To conclude, via this method, the UiO-66 synthesis was not adversely affected by the presence of dye. As dyed textiles constitute the majority of textile waste, this result provides evidence of a practical recycling method for converting textile waste into value-added MOF fabrics.

**Functional Stability of Catalytic Fabrics.** In Figure 7a, the DMNP degradation performance of  $\text{Zr@PET}_{\text{hyd}}$  upon repeated use was examined according to the DMNP conversion rate (%) per unit mass of fabric after reaction for 240 min of reaction. The performance of  $\text{Zr@PET}_{\text{hyd}}$  showed a slight decrease after four recycled uses; after the fourth recycling, the outcome was 80.1% compared to that of the first cycle. To examine the metal leaching from  $\text{Zr@PET}_{\text{hyd}}$ , 60 mg of  $\text{Zr@PET}_{\text{hyd}}$  was immersed in distilled water and vigorously stirred at 1100 rpm for 4 h. The water solution was then collected for analysis by ICP-MS. The concentration of Zr was as low as 0.61  $\mu\text{g/L}$ , confirming the stability of UiO-66 on

fibers.<sup>52</sup> For  $\text{Zr@PET}_{\text{hyd}}$  and  $\text{Zr+TA@PET}_{\text{hyd}}$ , which exhibited high catalytic performance, the functional stability after a harsh washing procedure was additionally tested, where washing with ethanol was conducted with stirring at 300 rpm for 24 h. Figure 7b shows the DMNP conversion rate (%) before and after the harsh washing process.  $\text{Zr+TA@PET}_{\text{hyd}}$  lost its catalytic capabilities considerably after washing, while  $\text{Zr@PET}_{\text{hyd}}$  maintained these capabilities. For  $\text{Zr+TA@PET}_{\text{hyd}}$ , the externally added TA reacted with metal ions, forming a thicker layer of UiO-66 than in the  $\text{Zr@PET}_{\text{hyd}}$  case. While this extra layer offered higher catalytic performance initially, the outer UiO-66 layer appeared to be weakly adhered to the surface, with a considerable number of particles falling off after the harsh washing. As a result, this sample showed significantly lower DMNP conversion performance capabilities. Because most of the UiO-66 on  $\text{Zr@PET}_{\text{hyd}}$  was directly attached to carboxyl groups on the hydrolyzed surface, the UiO-66 adherence was stronger for  $\text{Zr@PET}_{\text{hyd}}$ , meaning that it maintained higher catalytic performance even after harsh agitation. Following the harsh washing cycle, it was confirmed that the morphology of the UiO-66 crystals in  $\text{Zr@PET}_{\text{hyd}}$  remained intact (Figure S6a). An XRD analysis of  $\text{Zr@PET}_{\text{hyd}}$  conducted after the DMNP hydrolysis test indicated that the UiO-66 crystal structure was well maintained after the catalytic reaction (Figure S6b). Overall,  $\text{Zr@PET}_{\text{hyd}}$  exhibited an acceptable functional stability after harsh washing and repeated use, suggesting its practical applicability as an effective self-detoxifying material.

## CONCLUSIONS

This study presents a facile strategy for PET recycling that involves converting dyed PET fabric waste into a self-detoxifying fabric. PET template-based MOF synthesis assisted by acid hydrolysis and a DMF-solvothermal method was

explored for the simultaneous growth of UiO-66 directly onto a PET fabric and for the decolorization of the dyed PET fabric. In this approach, the PET surface was partially hydrolyzed to expose carboxyl groups, and metal ions were treated to bond with the carboxyl groups on the surface, forming UiO-66. The dye on the fabric decomposed during acidic hydrolysis, and the residual dye molecules were eliminated by a subsequent treatment by DMF. The effects of process variations on the morphology of the UiO-66-grown fabrics were investigated, as were their subsequent impact on the degradation of a nerve agent simulant, dimethyl 4-nitrophenyl phosphate (DMNP).

Intriguingly, the hydrolyzed PET treated only with Zr ions ( $\text{Zr@PET}_{\text{hyd}}$ ), displaying a thin and uniform coating of UiO-66, exhibited an accelerated DMNP degradation rate ( $t_{1/2} = 43.3$  min). PET fabrics treated with Zr ions and additional TA ( $\text{Zr+TA@PET}$ ) ( $t_{1/2} = 330$  min), which had a nonuniform coating but with a higher UiO-66 mass, showed a slower degradation rate. The  $\text{Zr+TA@PET}_{\text{hyd}}$  demonstrated greater MOF mass loading and the fastest half-life time for DMNP degradation ( $t_{1/2} = 14.5$  min). However, in practical applications,  $\text{Zr@PET}_{\text{hyd}}$  with the surface-assisted growth of UiO-66, appeared to better maintain its functional stability compared to  $\text{Zr+TA@PET}_{\text{hyd}}$ , implying that the bonding stability between the MOF and the PET surface may be a critical factor for sustaining continuous catalytic reactions.

This study demonstrates that through acid hydrolysis and a DMF-assisted solvothermal method, UiO-66 can be facilely synthesized on a dyed PET fabric. The developed material can serve as an effective protective material to detoxify organophosphorus CWAs. As dyed PET textiles constitute a substantial portion of PET waste, the findings from this research can provide an informative option for textile upcycling strategies to transform environmental waste into a value-added material, while also broadening the scope of PET recycling methods.

## ■ ASSOCIATED CONTENT

### SI Supporting Information

The Supporting Information is available free of charge at <https://pubs.acs.org/doi/10.1021/acsomega.3c09293>.

Figure S1: UiO-66 reaction system with fabrics; Figure S2: FE-SEM image and elemental mapping of  $\text{Zr@PET}_{\text{hyd}}$ ; Figure S3: PET fabrics after acid hydrolysis and DMF treatment for solvothermal synthesis of UiO-66; Table S1: dye removal (%) performance after acid hydrolysis and DMF treatment; Table S2: Hansen solubility parameters ( $\delta_D$ ,  $\delta_P$ ,  $\delta_H$ , and  $\delta_t$ ) and interaction radius  $R_0$  of DMF and PET fiber; Figure S4: kinetic analysis of DMNP degradation based on the first-order reaction kinetics for  $\text{Zr@PET}$ ,  $\text{Zr+TA@PET}$ ,  $\text{Zr@PET}_{\text{hyd}}$ ,  $\text{Zr+TA@PET}_{\text{hyd}}$ , and undyed  $\text{Zr@PET}_{\text{hyd}}$ ; Figure S5: BET  $\text{N}_2$  sorption–desorption isotherm of  $\text{Zr+TA@PET}_{\text{hyd}}$ ,  $\text{Zr+TA@PET}$ , and  $\text{Zr@PET}_{\text{hyd}}$ ; Table S3: zirconium elemental analysis by ICP-OES; Figure S6: FE-SEM image of  $\text{Zr@PET}_{\text{hyd}}$  after 24 h of ethanol washing and XRD patterns of  $\text{Zr@PET}_{\text{hyd}}$  after DMNP hydrolysis test (PDF)

## ■ AUTHOR INFORMATION

### Corresponding Author

Jooyoun Kim – Department of Fashion and Textiles and Research Institute of Human Ecology, Seoul National

University, Seoul 08826, Republic of Korea; [orcid.org/0000-0001-5043-9378](https://orcid.org/0000-0001-5043-9378); Email: [jkim256@snu.ac.kr](mailto:jkim256@snu.ac.kr)

### Authors

Seokhee Chang – Department of Fashion and Textiles, Seoul National University, Seoul 08826, Republic of Korea;

[orcid.org/0000-0002-9943-062X](https://orcid.org/0000-0002-9943-062X)

Soyeon Jin – Department of Fashion and Textiles, Seoul National University, Seoul 08826, Republic of Korea;

[orcid.org/0009-0003-4394-3420](https://orcid.org/0009-0003-4394-3420)

Complete contact information is available at:

<https://pubs.acs.org/10.1021/acsomega.3c09293>

### Author Contributions

The manuscript was written through contributions of all authors. All authors have given approval to the final version of the manuscript.

### Notes

The authors declare no competing financial interest.

## ■ ACKNOWLEDGMENTS

This work was supported by the National Research Foundation of Korea (NRF) grant funded by the Korea government (MSIT) (No. 2022R1A2C2003072).

## ■ REFERENCES

- (1) Dissanayake, D. G. K.; Weerasinghe, D. U. Fabric Waste Recycling: A Systematic Review of Methods, Applications, and Challenges. *Mater. Circ. Econ.* **2021**, *3*, 1–20.
- (2) Shanmugam, M.; Chuaicham, C.; Augustin, A.; Sasaki, K.; Sagayaraj, P. J. J.; Sekar, K. Upcycling Hazardous Metals and PET Waste-Derived Metal–Organic Frameworks: A Review on Recent Progresses and Prospects. *New J. Chem.* **2022**, *46*, 15776–15794.
- (3) Coates, G. W.; Getzler, Y. D. Y. L. Chemical Recycling to Monomer for an Ideal, Circular Polymer Economy. *Nat. Rev. Mater.* **2020**, *5*, 501–516.
- (4) Barnard, E.; Arias, J. J. R.; Thielemans, W. Chemolytic Depolymerisation of PET: A Review. *Green Chem.* **2021**, *23*, 3765–3789.
- (5) Boukayouht, K.; Bazzi, L.; El Hankari, S. Sustainable Synthesis of Metal–Organic Frameworks and Their Derived Materials from Organic and Inorganic Wastes. *Coord. Chem. Rev.* **2023**, *478*, No. 214986.
- (6) Dyosiba, X.; Ren, J.; Musyoka, N. M.; Langmi, H. W.; Mathe, M.; Onyango, M. S. Feasibility of Varied Polyethylene Terephthalate Wastes as a Linker Source in Metal–Organic Framework UiO-66 (Zr) Synthesis. *Ind. Eng. Chem. Res.* **2019**, *58*, 17010–17016.
- (7) Deleu, W. P. R.; Stassen, I.; Jonckheere, D.; Ameloot, R.; De Vos, D. E. Waste PET (bottles) as a Resource or Substrate for MOF Synthesis. *J. Mater. Chem. A* **2016**, *4*, 9519–9525.
- (8) Wang, Y.; Chen, L.; Hou, C.-C.; Wei, Y.-S.; Xu, Q. Multiple Catalytic Sites in MOF-Based Hybrid Catalysts for Organic Reactions. *Org. Biomol. Chem.* **2020**, *18*, 8508–8525.
- (9) Semrau, A. L.; Stanley, P. M.; Urstoeger, A.; Schuster, M.; Cokoja, M.; Fischer, R. A. Substantial Turnover Frequency Enhancement of MOF Catalysts by Crystallite Downsizing Combined with Surface Anchoring. *ACS Catal.* **2020**, *10*, 3203–3211.
- (10) Ma, X.; Chai, Y.; Li, P.; Wang, B. Metal–Organic Framework Films and Their Potential Applications in Environmental Pollution Control. *Acc. Chem. Res.* **2019**, *52*, 1461–1470.
- (11) Kalinovsky, Y.; Cooper, N. J.; Main, M. J.; Holder, S. J.; Blight, B. A. Microwave-Assisted Activation and Modulator Removal in Zirconium MOFs for Buffer-Free CWA Hydrolysis. *Dalton Trans.* **2017**, *46*, 15704–15709.
- (12) Dwyer, D. B.; Lee, D. T.; Boyer, S.; Bernier, W. E.; Parsons, G. N.; Jones, W. E., Jr. Toxic Organophosphate Hydrolysis Using

Nanofiber-Templated UiO-66-NH<sub>2</sub> Metal–Organic Framework Polycrystalline Cylinders. *ACS Appl. Mater. Interfaces* **2018**, *10*, 25794–25803.

(13) Kirlikovali, K. O.; Chen, Z.; Islamoglu, T.; Hupp, J. T.; Farha, O. K. Zirconium-Based Metal–Organic Frameworks for the Catalytic Hydrolysis of Organophosphorus Nerve Agents. *ACS Appl. Mater. Interfaces* **2020**, *12*, 14702–14720.

(14) Plonka, A. M.; Grissom, T. G.; Musaev, D. G.; Balboa, A.; Gordon, W. O.; Collins-Wildman, D. L.; Ghose, S. K.; Tian, Y.; Ebrahim, A. M.; Mitchell, M. B.; Hill, C. L.; Morris, J. R.; Frenkel, A. I. Effect of Carbon Dioxide on the Degradation of Chemical Warfare Agent Simulant in the Presence of Zr Metal Organic Framework MOF-808. *Chem. Mater.* **2019**, *31*, 9904–9914.

(15) Islamoglu, T.; Ortuño, M. A.; Proussaloglou, E.; Howarth, A. J.; Vermeulen, N. A.; Atilgan, A.; Asiri, A. M.; Cramer, C. J.; Farha, O. K. Presence versus Proximity: The Role of Pendant Amines in the Catalytic Hydrolysis of a Nerve Agent Simulant. *Angew. Chem., Int. Ed.* **2018**, *57*, 1949–1953.

(16) Yang, T.; Ma, T.; Yang, L.; Dai, W.; Zhang, S.; Luo, S. A Self-Supporting UiO-66 Photocatalyst with Pd Nanoparticles for Efficient Degradation of Tetracycline. *Appl. Surf. Sci.* **2021**, *544*, No. 148928.

(17) Abdelhameed, R. M.; Rehan, M.; Emam, H. E. Figuration of Zr-Based MOF@Cotton Fabric Composite for Potential Kidney Application. *Carbohydr. Polym.* **2018**, *195*, 460–467.

(18) Xu, T.; Zhang, Y.; Liu, M.; Wang, H.; Ren, J.; Tian, Y.; Liu, X.; Zhou, Y.; Wang, J.; Zhu, W.; Ma, M. In-Situ Two-Step Electrodeposition of  $\alpha$ -CD-rGO/Ni-MOF Composite Film for Superior Glucose Sensing. *J. Alloys Compd.* **2022**, *923*, No. 166418.

(19) Balasubramanian, S.; Kulandaisamy, A. J.; Babu, K. J.; Das, A.; Balaguru Rayappan, J. B. Metal Organic Framework Functionalized Textiles as Protective Clothing for the Detection and Detoxification of Chemical Warfare Agents—A Review. *Ind. Eng. Chem. Res.* **2021**, *60*, 4218–4239.

(20) Ma, K.; Idrees, K. B.; Son, F. A.; Maldonado, R.; Wasson, M. C.; Zhang, X.; Wang, X.; Shehayeb, E.; Merhi, A.; Kaafarani, B. R.; Islamoglu, T.; Xin, J. H.; Farha, O. K. Fiber Composites of Metal–Organic Frameworks. *Chem. Mater.* **2020**, *32*, 7120–7140.

(21) Sun, X.-H.; Chen, S.-H.; Guo, Q.-Z.; Shen, Z.-C.; Wu, J.; Du, Z.-X. Convenient Recycling and Efficient Photocatalytic Degradation of Disinfection By-Products by In-Situ Growth MOF on PET. *Sep. Purif. Technol.* **2023**, *324*, No. 124506.

(22) Semyonov, O.; Chaemchuen, S.; Ivanov, A.; Verpoort, F.; Kolska, Z.; Syrtanov, M.; Svorcik, V.; Yusubov, M. S.; Lyutakov, O.; Guselnikova, O.; Postnikov, P. S. Smart Recycling of PET to Sorbents for Insecticides through In Situ MOF Growth. *Appl. Mater. Today* **2021**, *22*, No. 100910.

(23) Semyonov, O.; Kogolev, D.; Mamontov, G.; Kolobova, E.; Trelin, A.; Yusubov, M. S.; Guselnikova, O.; Postnikov, P. S. Synergetic Effect of UiO-66 and Plasmonic AgNPs on PET Waste Support towards Degradation of Nerve Agent Simulant. *Chem. Eng. J.* **2022**, *431*, No. 133450.

(24) Kogolev, D.; Semyonov, O.; Metalnikova, N.; Fatkullin, M.; Rodriguez, R. D.; Slepicka, P.; Yamauchi, Y.; Guselnikova, O.; Boukherroub, R.; Postnikov, P. S. Waste PET Upcycling to Conductive Carbon-Based Composite through Laser-Assisted Carbonization of UiO-66. *J. Mater. Chem. A* **2023**, *11*, 1108–1115.

(25) Torres-Cortés, S. A.; Velasquez, M.; Pérez, L. D.; Sierra, C. A. Ex Situ Synthesis of MOF@PET/Cotton Textile Fibers as Potential Antibacterial Materials. *J. Polym. Res.* **2022**, *9*, 427.

(26) Planas, N.; Mondloch, J. E.; Tussupbayev, S.; Borycz, J.; Gagliardi, L.; Hupp, J. T.; Farha, O. K.; Cramer, C. J. Defining the Proton Topology of the Zr<sub>6</sub>-Based Metal–Organic Framework NU-1000. *J. Phys. Chem. Lett.* **2014**, *5*, 3716–3723.

(27) Li, Y.; Yi, H.; Li, M.; Ge, M.; Yao, D. Synchronous Degradation and Decolorization of Colored Poly (ethylene terephthalate) Fabrics for the Synthesis of High Purity Terephthalic Acid. *J. Clean. Prod.* **2022**, *366*, No. 132985.

(28) Ploskonka, A. M.; DeCoste, J. B. Insight into Organophosphate Chemical Warfare Agent Simulant Hydrolysis in Metal–Organic Frameworks. *J. Hazard. Mater.* **2019**, *375*, 191–197.

(29) Katz, M. J.; Klet, R. C.; Moon, S.-Y.; Mondloch, J. E.; Hupp, J. T.; Farha, O. K. One Step Backward is Two Steps Forward: Enhancing the Hydrolysis Rate of UiO-66 by Decreasing [OH<sup>-</sup>]. *ACS Catal.* **2015**, *5*, 4637–4642.

(30) Golshaei, P.; Güven, O. Chemical Modification of PET Surface and Subsequent Graft Copolymerization with Poly (N-isopropylacrylamide). *React. Funct. Polym.* **2017**, *118*, 26–34.

(31) Rosmaninho, M. G.; Jardim, E.; Moura, F. C. C.; Ferreira, G. L.; Thom, V.; Yoshida, M. I.; Araujo, M. H.; Lago, R. M. Surface Hydrolysis of Postconsumer Polyethylene Terephthalate to Produce Adsorbents for Cationic Contaminants. *J. Appl. Polym. Sci.* **2006**, *102*, 5284–5291.

(32) Wang, Y.; Zhang, Y.; Song, H.; Wang, Y.; Deng, T.; Hou, X. Zinc-Catalyzed Ester Bond Cleavage: Chemical Degradation of Polyethylene Terephthalate. *J. Clean. Prod.* **2019**, *208*, 1469–1475.

(33) Yao, L.; Zhang, S.; Wang, R.; Zhang, L.; Wang, Y.; Yin, W. Phosphoric Acid Functionalized Superhydrophilic and Underwater Superoleophobic UiO-66/Polyester Fabric Composite Membrane for Efficient Oil/Water Separation and Gd (III) Recovery. *Desalination* **2022**, *544*, No. 116141.

(34) Chen, W.; McCarthy, T. J. Chemical Surface Modification of Poly (ethylene terephthalate). *Macromolecules* **1998**, *31*, 3648–3655.

(35) Majumder, M.; Keis, K.; Zhan, X.; Meadows, C.; Cole, J.; Hinds, B. J. Enhanced Electrostatic Modulation of Ionic Diffusion through Carbon Nanotube Membranes by Diazonium Grafting Chemistry. *J. Membr. Sci.* **2008**, *316*, 89–96.

(36) Garcia-Fernandez, M. J.; Martinez-Calvo, L.; Ruiz, J. C.; Wertheimer, M. R.; Concheiro, A.; Alvarez-Lorenzo, C. Loading and Release of Drugs from Oxygen-Rich Plasma Polymer Coatings. *Plasma Processes Polym.* **2012**, *9*, 540–549.

(37) Lee, D. T.; Zhao, J.; Oldham, C. J.; Peterson, G. W.; Parsons, G. N. UiO-66-NH<sub>2</sub> Metal–Organic Framework (MOF) Nucleation on TiO<sub>2</sub>, ZnO, and Al<sub>2</sub>O<sub>3</sub> Atomic Layer Deposition-Treated Polymer Fibers: Role of Metal Oxide on MOF Growth and Catalytic Hydrolysis of Chemical Warfare Agent Simulants. *ACS Appl. Mater. Interface* **2017**, *9*, 44847–44855.

(38) Van Le, D.; Nguyen, M. B.; Dang, P. T.; Lee, T.; Nguyen, T. D. Synthesis of a UiO-66/gC<sub>3</sub>N<sub>4</sub> Composite Using Terephthalic Acid Obtained from Waste Plastic for the Photocatalytic Degradation of the Chemical Warfare Agent Simulant, Methyl Paraoxon. *RSC Adv.* **2022**, *12*, 22367–22376.

(39) Biswas, P.; Shuster, D. B.; Sonmez Baghirzade, B.; Scanga, R. A.; Harris, S. A.; Tran, C. N.; Apul, O. G.; Reuther, J. F. Oxime-Functionalized, Nonwoven Nanofabrics for Rapid, Inexpensive Decontamination of a Nerve Agent Simulant. *ACS Appl. Nano Mater.* **2023**, *6*, 3425–3434.

(40) Zhao, J.; Gong, B.; Nunn, W. T.; Lemaire, P. C.; Stevens, E. C.; Sidi, F. I.; Williams, P. S.; Oldham, C. J.; Walls, H. J.; Shepherd, S. D.; Browe, M. A.; Peterson, G. W.; Losego, M. D.; Parsons, G. N. Conformal and Highly Adsorptive Metal–Organic Framework Thin Films via Layer-By-Layer growth on ALD-Coated Fiber Mats. *J. Mater. Chem. A* **2015**, *3*, 1458–1464.

(41) DeStefano, M. R.; Islamoglu, T.; Garibay, S. J.; Hupp, J. T.; Farha, O. K. Room-Temperature Synthesis of UiO-66 and Thermal Modulation of Densities of Defect Sites. *Chem. Mater.* **2017**, *29*, 1357–1361.

(42) Chen, X.; Li, Y.; Fu, Q.; Qin, H.; Lv, J.; Yang, K.; Zhang, Q.; Zhang, H.; Wang, M. An Efficient Modulated Synthesis of Zirconium Metal–Organic Framework UiO-66. *RSC Adv.* **2022**, *12*, 6083–6092.

(43) Siddique, M.; Farooq, R.; Khalid, A.; Farooq, A.; Mahmood, Q.; Farooq, U.; Raja, I. A.; Shaikat, S. F. Thermal-Pressure-Mediated Hydrolysis of Reactive Blue 19 Dye. *J. Hazard. Mater.* **2009**, *172*, 1007–1012.

(44) Mu, B.; Yang, Y. Complete Separation of Colorants from Polymeric Materials for Cost-Effective Recycling of Waste Textiles. *J. Chem. Eng.* **2022**, *427*, No. 131570.

(45) Song, L.; Zhao, T.; Yang, D.; Wang, X.; Hao, X.; Liu, Y.; Zhang, S.; Yu, Z.-Z. Photothermal Graphene/UiO-66-NH<sub>2</sub> Fabrics for Ultrafast Catalytic Degradation of Chemical Warfare Agent Simulants. *J. Hazard. Mater.* **2020**, *393*, No. 122332.

(46) Yang, J.; He, X.; Dai, J.; Tian, R.; Yuan, D. Photo-Assisted Enhancement Performance for Rapid Detoxification of Chemical Warfare Agent Simulants over Versatile ZnIn<sub>2</sub>S<sub>4</sub>/UiO-66-NH<sub>2</sub> Nanocomposite Catalysts. *J. Hazard. Mater.* **2021**, *417*, No. 126056.

(47) Zhou, M.; Zou, W.; Zhu, X.; Ma, H.; Wang, P.; Shang, J.; Luo, P. In Situ Growth of UiO-66-NH<sub>2</sub> on Thermally Stabilized Electrospun Polyacrylonitrile Nanofibers for Visible-Light Driven Cr(VI) Photocatalytic Reduction. *J. Solid State Chem.* **2022**, *307*, No. 122836.

(48) Gibbons, B.; Bartlett, E. C.; Cai, M.; Yang, X.; Johnson, E. M.; Morris, A. J. Defect Level and Particle Size Effects on the Hydrolysis of a Chemical Warfare Agent Simulant by UiO-66. *Inorg. Chem.* **2021**, *60*, 16378–16387.

(49) Katz, M. J.; Mondloch, J. E.; Totten, R. K.; Park, J. K.; Nguyen, S. T.; Farha, O. K.; Hupp, J. T. Simple and Compelling Biomimetic Metal–Organic Framework Catalyst for the Degradation of Nerve Agent Simulants. *Angew. Chem., Int. Ed.* **2014**, *126*, 507–511.

(50) Hu, Q.; Wang, X.; Zheng, Y.; Zhao, T.; Qu, J.; Yu, Z.-Z.; Yang, D. Solar-Thermally Enhanced Catalytic Hydrolysis of Chemical Warfare Agent Simulant with UiO-66-NCS Decorated Reduced Graphene Oxide Aerogels. *J. Chem. Eng.* **2023**, *476*, No. 146606.

(51) Lee, D. T.; Dai, Z.; Peterson, G. W.; Hall, M. G.; Pomerantz, N. L.; Hoffman, N.; Parsons, G. N. Highly Breathable Chemically Protective MOF-Fiber Catalysts. *Adv. Funct. Mater.* **2022**, *32*, No. 2108004.

(52) Zhao, J.; Lee, D. T.; Yaga, R. W.; Hall, M. G.; Barton, H. F.; Woodward, I. R.; Oldham, C. J.; Walls, H. J.; Peterson, G. W.; Parsons, G. N. Ultra-Fast Degradation of Chemical Warfare Agents Using MOF–Nanofiber Kebabs. *Angew. Chem., Int. Ed.* **2016**, *128*, 13418–13422.